



Selective hydrogenation of acetic acid to ethanol on Cu-In catalyst supported by SBA-15



Xiuqin Dong^{a,b}, Junwei Lei^{a,b}, Yifei Chen^{a,b}, Haoxi Jiang^{a,b}, Minhua Zhang^{a,b,*}

^a Key Laboratory for Green Chemical Technology of Ministry of Education, R&D Center for Petrochemical Technology, Tianjin University, Tianjin, 300072, China

^b Collaborative Innovation Center of Chemical Science and Engineering, Tianjin, 300072, China

ARTICLE INFO

Keywords:

Acetic acid hydrogenation
Cu-In alloy
Ethanol

ABSTRACT

The supported copper based catalysts could be potential candidate for the selective catalytic hydrogenation of acetic acid to produce ethanol instead of noble metals. In this work, a series of highly efficient bimetallic Cu-In/SBA-15 catalysts were designed and prepared via the deposition-precipitation method. Detailed characterizations were carried out to investigate the textural properties, dispersion and chemical state of the metals, the interactions between copper and indium species, the adsorption and activation of acetic acid on the catalysts surface. The results clearly demonstrated the coexistence of Cu-In alloy and metallic Cu under the reductive reaction atmosphere. The strong synergistic effect inside Cu-In alloy not only accelerated the dissociation of acetic acid to acetate, but also hindered the combination of acetyl and ethoxy species to form ethyl acetate, thus promoting the catalytic hydrogenation performance significantly. It was also found that the concentration of adsorbed H atoms on catalysts was one of the indispensable factors affecting the ethanol selectivity, which was positively correlated to the exposed Cu surface area and H₂ partial pressure. The optimal catalytic hydrogenation activity was obtained for 9Cu1In/SBA-15 under the reaction conditions of 2.5 MPa and 623 K, the conversion of acetic acid and selectivity of ethanol reached 99.1% and 90.9%, respectively. These results might provide an inspiration in the rational design of novel copper based catalysts for carboxylic acid hydrogenation.

1. Introduction

Ethanol is an important fundamental commodity feedstock for its widely application in food and industry. It can be subsequently converted to ethylene, polyethylene, vinyl acetate and ethyl acetate or any of a wide variety of other chemical products [1,2]. Besides, renewable ethanol may be used as a potential environmentally benign gasoline additive to alleviate the dependence on petroleum-derived fuels, increasing energy security and contributing to the environmental protection. It has been reported that automotive fuels consisting of 10–40% ethanol are greatly encouraged in America and Brazil. By 2020, the traditional gasoline will be gradually replaced by E10 ethanol gasoline (consisted of 10% ethanol and 90% gasoline) throughout China, thus the demand for ethanol will increase dramatically.

Acetic acid is largely over produced by the homogeneous catalytic carbonylation process of methanol under mild operating conditions [3,4], benefiting from the rapid development of coal chemical industry in China. Therefore, it is urgent to develop new downstream products starting from acetic acid. Considering the theoretical and economic

feasibility, the acetic acid could be selectively hydrogenated to ethanol in the presence of metal catalyst, and at the same time, as an alternative technology to fermentation to meet the increasingly demand of ethanol [5].

Over the past decades, the study on the catalysts for ethanol production via acetic acid reduction has attracted extensively attentions. The catalysts for acetic acid hydrodeoxygénéation typically comprised of one or more noble metals of group VIII and a second transition metal as promoter dispersed on the oxides of group IIIA or IVA elements [6]. Currently, reported catalysts based on the density functional theory and experiments for selective reduction of acetic acid in vapor or aqueous phase mainly consist of Pt [7–11], Pd [12], Ru [13–16], Rh [17] and other precious metals [18]. These noble metal based catalysts have been proved to show excellent catalytic performance and some of them have realized industrialization in many countries in recent years [19]. However, high price and limited resources of precious metals have limited their large scale industrial application. Therefore, the development of novel low cost catalyst with high activity and selectivity is urgently needed for acetic acid hydrogenation to ethanol.

* Corresponding author at: Key Laboratory for Green Chemical Technology of Ministry of Education, R&D Center for Petrochemical Technology, Tianjin University, Tianjin, 300072, China.

E-mail address: mhzhang@tju.edu.cn (M. Zhang).

It was reported that copper containing catalysts were in favor of selective hydrogenation of carbon-oxygen bonds, but were relatively inactive in carbon-carbon bond hydrogenolysis [20]. They could be promising candidates for hydrogenation processes, such as selective hydroconversion of esters and carboxylic acids to alcohols [21,22], CO or CO_2 catalytic hydrogenation to methanol or ethanol [23], glycerol hydrogenolysis to produce 1,2-propanediol [24,25]. Most importantly, the hydrodecarbonylation process is significantly inhibited. However, the activity, sinter-resistant and/or mechanically stability for copper itself could not fully meet the requirements of industrial applications for the hydrogenation of acetic acid [20]. DFT studies also showed that the monometallic copper catalysts were less active in dissociative adsorption of acetic acid through cleavage of C–O bond adjacent to the carbonyl group, which could be the rate control step in the hydrogenation of acetic acid to ethanol [19,22]. Conventionally, the bimetallic catalysts usually showed distinct properties when compared with those monometallic catalysts and exhibited enhanced activity, selectivity and stability. Onyestyak et al. [6,26–29] discovered that Cu_2In alloy could be formed, when doping indium atoms on the supported Cu catalysts, leading to significant improvement of activity and selectivity in the reduction of acetic acid to ethanol, or octanoic acid to octanol. Indium was also found to be strikingly efficient in inhibiting carbon atom loss by hydro-decarbonylation for supported platinum and nickel catalysts [30]. In our group's previous work, the mechanism of acetic acid hydrogenation on $\text{Cu}_2\text{In}(100)$ plane was investigated through DFT calculations, and the most likely reaction route from acetic acid to ethanol was in the following order: $\text{CH}_3\text{COOH} \rightarrow \text{CH}_3\text{COO} \rightarrow \text{CH}_3\text{CHOO} \rightarrow \text{CH}_3\text{CHO} \rightarrow \text{CH}_3\text{CH}_2\text{O} \rightarrow \text{CH}_3\text{CH}_2\text{OH}$ [31]. However, the detailed mechanism, how indium helps to improve catalytic performance as a chemical contributor in the hydrogenation of acetic acid, was not confirmed by experiment.

In present work, SBA-15 was chose as the support because of its excellent hydrothermally stability and unique physical properties (larger specific surface area and pore volume, highly ordered mesopores, thicker pore wall). The deposition precipitation technique was adopted as preparation method, taking its advantages of excellent performance in dispersion, loading degree, thermochemical stability and catalytic activity of nanoparticles [32]. A series of highly dispersed monometallic and bimetallic copper-indium catalysts were prepared via the deposition precipitation with Na_2CO_3 as alkaline precipitant, and they were tested for the synthesis of ethanol from acetic acid hydrogenation. The CuIn/SBA-15 catalyst with optimized Cu/In ratio showed excellent catalytic performance in the hydrogenation of acetic acid. The effects of indium doping on the structure and physicochemical properties were systematically studied by XRD, H_2 -TPR, TEM, XPS, N_2O chemisorption, in-situ DRIFTS techniques. The possible detailed mechanism of acetic acid hydrogenation on Cu-In bimetallic catalyst was also discussed.

2. Experimental

2.1. Catalyst preparation

The SBA-15 supported copper based catalyst samples were prepared by deposition-precipitation with Na_2CO_3 aqueous solution as precipitant [32]. Briefly, commercial SBA-15 (purchased from Nanjing XFNANO Materials Tech Co., Ltd, China) was firstly calcined (at 823 K for 6 h in air) to eliminate possible organic contaminants, and then dispersed in 0.14 M copper and indium nitrates aqueous solution ($\text{Cu}(\text{NO}_3)_2 \cdot 3\text{H}_2\text{O}$ and $\text{In}(\text{NO}_3)_3$ with different ratios) at a constant temperature of 333 K. The suspension was vigorously stirred for 30 min. Then 0.16 M Na_2CO_3 aqueous solution was added dropwise until the pH value reached 7.5 ± 0.2 and then stirred for 2 h. The light blue precipitate was separated by filtration, washed with deionized water, and then dried in air at 373 K overnight. Finally, the dried sample was calcined in a muffle oven at 723 K for 4 h with a heating rate of 2 K/

min. The obtained catalyst sample was denoted as $x\text{CuIn/SBA-15}$, where x and y were referred to the nominal weight ratios of copper and indium in the base of support, respectively.

2.2. Catalyst characterization

N_2 physical adsorption-desorption isotherms measurements were conducted at 77 K with a Micromeritics Tristar 3000 analyzer. Before the measurement, the samples were outgassed under vacuum at 573 K for 6 h to remove any possible physically adsorbed impurities. The specific surface area was calculated by the BET (Brunauer-Emmett-Teller) method. The pore size distribution was derived from the desorption branch of isotherm adopting the nonlocal density functional theory (NL-DFT) for cylindrical pores.

Powder X-ray diffraction (XRD) patterns were recorded on Rigaku MiniFlex 600 X-ray diffractometer with $\text{Cu-K}\alpha$ radiation (40 kV and 15 mA) in the step mode (0.02°, 0.06 s). And the scanning angle (2θ) range was from 10 to 80°. The crystallite phase was identified by using JCPDS database as references. The mean crystallite size of metal particle was calculated by the Scherrer equation using full width at half maximum.

Transmission electron microscopy (TEM) was performed on a FEI Tecnai G2 F20 field-emission electron microscope operated at an acceleration voltage of 200 kV. The catalysts were firstly grounded, and then ultrasonically dispersed in ethanol for at least 1 h. The as-prepared suspension was dropped on Mo grid coated with carbon film. EDX was used as a supplementary mean for composition analysis.

Actual metal contents in the final catalysts were determined by a Varian Vista-MPX inductively coupled plasma optical emission spectrometry (ICP-OES) operated at high frequency emission power of 1.5 kW and plasma air flow rate of 15.0 ml/min. The samples were firstly dissolved in the mixture of HF, *aqua regia* and H_3BO_3 , then the solution was diluted to a fixed volume.

Temperature-programmed reduction (H_2 -TPR) was performed on a Micromeritics Autochem II 2920 adsorption analyzer equipped with a TCD to study the reducibility and the extent of reduction of the samples. About 50 mg catalyst was loaded in a U-shaped quartz tube and pretreated in an Ar flow at 673 K for 2 h to remove the surface impurities, then the sample was cooled down to 323 K. Afterwards, the catalyst was heated to 873 K in 10% H_2 -90% Ar flow with a heating rate of 5 K/min. A cold trap was stalled to condense water out of the gases before they flow through the detector. The amount of hydrogen consumption was recorded by TCD.

Hydrogen chemisorption was carried out on a Micromeritics ASAP 2020 automated adsorption analyzer. The sample was reduced in 10% H_2 -90% Ar flow at 623 K for 1 h, and outgassed under vacuum for 1 h to remove chemisorbed hydrogen species completely. H_2 adsorption isotherm was measured in a hydrogen pressure ranging from 0 to 760 mmHg at 77 K. Then evacuation was conducted again to remove the reversibly adsorbed hydrogen on the surface of catalyst before a second isotherm was performed under the same conditions as the first one. The amounts of total and reversible adsorbed H_2 were obtained by extrapolating the first and second hydrogen adsorption isotherm to zero pressure, respectively [33]. The quantity of irreversibly chemisorbed hydrogen was the difference between total and reversible adsorbed hydrogen.

Dissociative N_2O chemisorption was applied to determine the metallic copper surface areas and dispersion on a Micromeritics Autochem II 2920 analyzer, using the procedure described by Van Der Grift et al. [34]. Briefly, 100 mg catalyst was reduced in 10% H_2 -90% Ar flow at 623 K for 2 h, and then cooled down to 323 K in Ar atmosphere. Then the surface metallic copper species was completely oxidized to Cu_2O based on the stoichiometry of reaction ($2\text{Cu} + \text{N}_2\text{O} \rightarrow \text{Cu}_2\text{O} + \text{N}_2$) by introducing a flow of 10% N_2O -90% Ar for 1 h. The residual N_2O was purged out with a flow of high-purity Ar for 1 h. Finally, another H_2 -TPR experiment was performed as described above. The peaks ascribed

to the reduction of Cu_2O and In_2O_3 were independent of each other in the second H_2 -TPR profile. And the amount of hydrogen consumption for Cu_2O reduction was quantified by a calibrated TCD. However, as it was hard to distinguish the hydrogen consumption of copper from that of indium in the first H_2 -TPR profile, the hydrogen consumption for reduction of all copper atoms was calculated from ICP data. Copper dispersion was calculated by dividing the amount of surface copper atom by the total number of supported copper atoms. The exposed copper surface area was expressed in the form of copper surface area per unit mass of catalyst ($\text{m}^2\text{-Cu/g-cat.}$).

X-ray photoelectron spectra (XPS) was carried out on a PHI 1600 ESCA instrument (PE company) coupled with an $\text{Al K}\alpha$ X-ray radiation source ($\hbar\nu = 1486.6$ eV) at a pressure of $< 1 \times 10^{-6}$ Torr. Prior to the measurement, the catalyst was firstly reduced at 623 K in 10% H_2 -90%Ar flow for 2 h. Then the reduced catalyst was protected by ultra-high purity nitrogen and transferred onto the sample holder using a glove box. Finally, the sample holder was transferred into the XPS chamber. The specific photoelectron energy region of each element was repeatedly scanned to get good signal-to-noise ratios. The whole procedure was operated carefully to avoid exposure to air as far as possible. The binding energy was calibrated using C1s (284.5 eV) peak as reference.

In-situ DRIFTS of acetic acid adsorption and acetic acid hydrogenation were performed to discern the nature of the adsorbed species on the catalysts on a Nicolet 6700 spectrometer coupled with a high-temperature DRIFTS cell, fitted with a ZnSe window. The catalyst was firstly reduced in situ at 623 K in 10% H_2 -90%Ar flow for 2 h under atmospheric pressure and purged with high-purity N_2 . Then the reduced catalyst was evacuated under high vacuum ($< 10^{-3}$ Pa) to eliminate any possible impurities, especially physically adsorbed water. The background spectra at different temperature were recorded when the sample was cooled down to ambient temperature. The adsorption of acetic acid was conducted at room temperature by passing N_2 stream through a glass vessel containing acetic acid under pressure of 0.1 MPa. After the catalyst was saturated with acetic acid, the system was purged again with N_2 stream for 1 h to remove the physically adsorbed acetic acid. Infrared spectra of adsorbed species were recorded at a resolution of 4 cm^{-1} .

Then pure hydrogen flow (99.99%, 30 ml/min) was introduced into the system, the infrared spectra at varied temperatures were recorded at a resolution of 4 cm^{-1} and referenced to the background at corresponding temperature.

2.3. Catalytic activity test

The activity test for selective hydrogenation of acetic acid was carried out in a continuously operated fixed bed reactor with an inner diameter of 10.0 mm. Approximately 0.9 g fresh catalyst sample (40–60 meshes) was loaded into the isothermal region of the stainless steel tubular reactor. Prior to initiating the reaction, the catalysts were firstly reduced in 10% H_2 -90% Ar atmosphere at 623 K for 4 h with a ramping rate of 5 K/min (10In/SBA-15 was reduced at 823 K for 4 h). Then pure H_2 was fed into the reaction system, and the system pressure was raised to 2.5 MPa by regulating back-pressure valve and pressure reducing valve. Acetic acid was pumped into the system through a high pressure pump (SSI, LS class) and vaporized in the preheating section of reactor. The effluent was condensed by a cold trap coupled with a thermostatic water bath. The condensed liquid phase of the reaction product was analyzed on a Shimadzu GC-2010 plus gas chromatograph equipped with a flame ionization detector and a RTX-Wax capillary column (RESTEK, 30 m \times 0.32 mm \times 0.25 μm). The gas phase of the product was analyzed for CO_2 , CH_4 , CO and light hydrocarbons on another Shimadzu GC-2010 plus gas chromatograph equipped with a thermal conductivity detector and a Carboxen 1006 Plot capillary column (RESTEK, 30 m \times 0.32 mm \times 0.25 μm). The conversion of acetic acid and selectivity of specific products were calculated based on the carbon

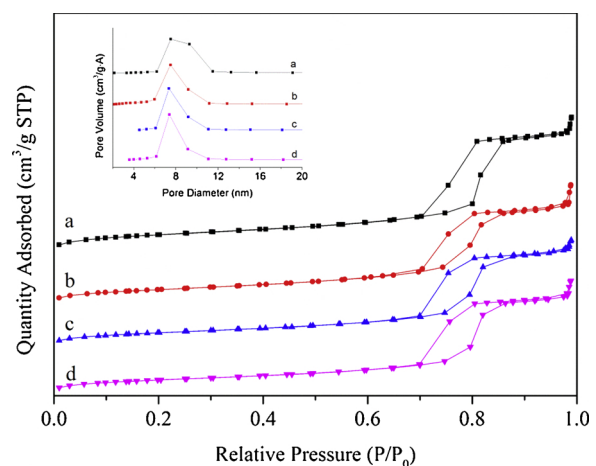


Fig. 1. N_2 adsorption-desorption isotherms at 77 K and pore size distributions (inset figure): (a) SBA-15, (b) 10Cu/SBA-15, (c) 9Cu1In/SBA-15 and (d) 10In/SBA-15.

mass balance.

3. Results and discussion

3.1. N_2 -adsorption

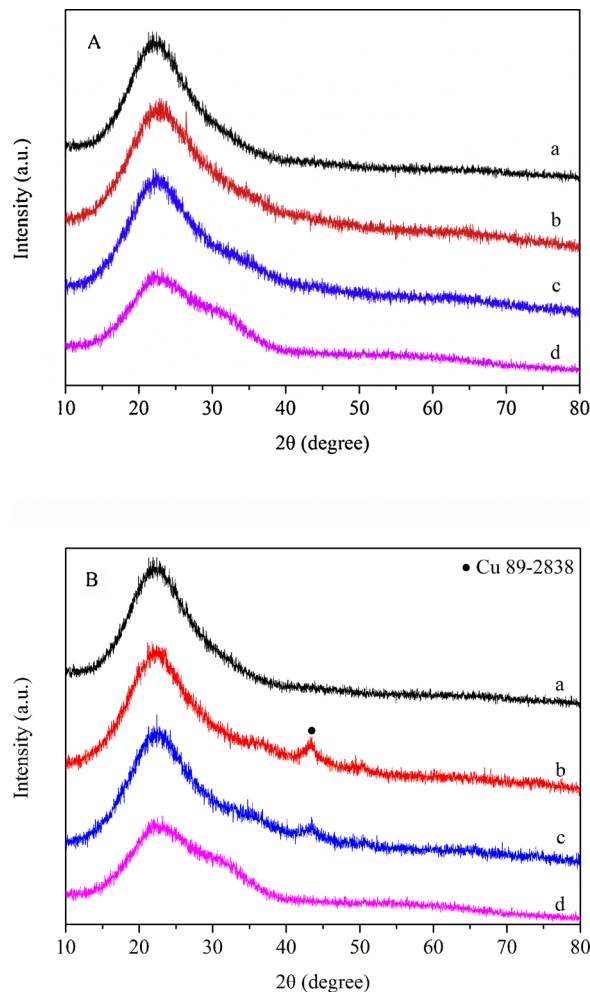
The textural properties of SBA-15 samples before and after loading of copper and indium species were assessed by nitrogen physisorption at 77 K. The corresponding adsorption-desorption isotherms and pore size distribution curves of SBA-15, 10Cu/SBA-15, 9Cu1In/SBA-15 and 10In/SBA-15 were shown in Fig. 1. It could be observed that all the samples exhibited similar type of isotherms. According to IUPAC standard, the isotherms were classified as Langmuir type IV with a clear type-H1 hysteresis loop, which was characteristic of porous materials with uniform and open cylindrical mesopores [35], in well agreement with TEM observation result. It was obvious that SBA-15 still retained its inherent mesoporous structure after loading with active metals. However, there were still some subtle differences between the parent SBA-15 and the supported copper-indium based materials. Nitrogen adsorption quantities of all samples were nearly the same when relative pressure P/P_0 was below 0.7, while supported catalysts adsorbed less N_2 than the parent SBA-15 at the relative pressure over 0.7. As a consequence, the H1 type hysteresis loops of supported catalysts were caused by capillary condensation effect, seemed to be a little flatter when compared with that of original SBA-15, indicating a decreased mesoporosity. This phenomenon was mainly attributed to the cavitation effect caused by partial blockage of initial mesopores and the emergence of ink-bottle shape mesopores [36,37].

Based on the isotherms displayed in Fig. 1, the textural properties of corresponding samples were evaluated using specific algorithms and summarized in Table 1. The total specific surface area and total pore volume of supported catalysts were around 20% lower than those of fresh SBA-15, while the micropore surface area and corresponding pore volume were barely changed. SBA-15 displayed a relatively wide pore size distribution in the range from 7.5 nm to 9.3 nm, whereas 10Cu/SBA-15, 9Cu1In/SBA-15 and 10In/SBA-15 presented analogous narrow pore size distributions with the extreme values centered at 7.5 nm, 7.4 nm and 7.3 nm, respectively. It could be inferred that the active metals tended to disperse homogeneously into the mesopores, leading to the slightly decrease of mesopores size and partial blockage in larger mesopores, which are in line with the corresponding adsorption/desorption isotherms. However, there was hardly any discrepancy among the supported catalysts, suggesting that the textural properties were not the decisive factor of catalytic performance.

Table 1

Textural properties of SBA-15 support and CuIn/SBA-15 samples.

Sample	$S_{\text{BET}}(\text{m}^2/\text{g})^{\text{a}}$	$S_{\text{micro}}(\text{m}^2/\text{g})^{\text{b}}$	$V_{\text{pore}}(\text{cm}^3/\text{g})^{\text{c}}$	$V_{\text{micro}}(\text{cm}^3/\text{g})^{\text{d}}$	$D_p(\text{nm})^{\text{e}}$
SBA-15	526	29	1.29	0.014	7.5;9.3
10Cu/SBA-15	444	24	1.07	0.010	7.5
9Cu1In/SBA-15	422	31	1.05	0.014	7.4
10In/SBA-15	413	24	1.05	0.011	7.3

^a S_{BET} : BET surface area.^b S_{micro} : t-Plot micropore surface area.^c V_{pore} : single point adsorption total pore volume at $p/p_0 = 0.97$.^d V_{micro} : t-Plot micropore volume.^e D_p average pore size evaluated by NL-DFT for cylindrical pores/equilibrium model.**Fig. 2.** XRD patterns of the calcined (A) and reduced (B) samples: (a) SBA-15, (b) 10Cu/SBA-15, (c) 9Cu1In/SBA-15 and (d) 10In/SBA-15.

3.2. XRD

Fig. 2 showed the XRD patterns of parent SBA-15 and the metal-loading samples. The diffraction line of parent SBA-15 displayed a single broad peak centered at 2θ of 23° , which was characteristic of amorphous silica. As shown in Fig. 2A, the typical reflections of SBA-15 were still retained in the calcined catalysts, and no new diffraction peak was detected, implying the homogeneously dispersion of metal species, which were believed to be mainly in the form of amorphous phyllosilicate [38]. The crystal structure of the reduced samples was illustrated in Fig. 2B. Apart from the obvious diffraction peak of silica, a weak peak ascribed to metallic copper (111) planes (JCPDS 89-2838) emerged at 2θ of 43° in the diffraction patterns of 10Cu/SBA-15 and

9Cu1In/SBA-15, indicating that the amorphous phyllosilicate was reduced at 623 K in 10% H_2 - 90% Ar flow. The reduced active metal species were dispersed homogeneously on the support, which could be confirmed by the following TEM observation.

3.3. TEM

The highly dispersion of active metal species was also confirmed by the TEM images of reduced 10Cu/SBA-15, 9Cu1In/SBA-15, 10In/SBA-15 samples and the parent SBA-15 in Fig. 3. As illustrated in Fig. 3a, SBA-15 exhibited highly ordered mesoporous channels with average diameter of approximately 7 nm , verifying the nitrogen physisorption results. As for these supported catalysts, the harsh catalyst preparation process, including vigorously stirring in alkaline condition, calcination at high temperature and reduction under hydrogen atmosphere, didn't cause structural damage to the support, the initial cylindrical mesopore of SBA-15 was still preserved on the supported catalysts. In addition, EDX analysis (not shown) indicated that the elemental composition in the described areas was close to the ICP result, but agglomerated metal particles were barely discerned on the surface or inside the channel. However, a kind of amorphous material with flaky structure was observed to be distributed evenly inside the channel, without causing the blockage of pore structure, implying the high dispersion degree of metal components, which was well consistent with the XRD characterization result.

3.4. H_2 -TPR

H_2 -TPR profiles of the representative calcined samples with different copper and indium contents were illustrated in Fig. 4A. Pure CuO powder was taken as a reference. A single peak centered at 494 K was observed for the complete reduction of bulk CuO to metallic Cu. When copper was loaded on SBA-15, only one sharp peak centered at 471 K was detected in 10Cu/SBA-15, which was attributed to the reduction of highly dispersed copper species. Meanwhile, the reduction of In/SBA-15 was much more difficult compared to the pure copper supported catalyst. There was a rather broad peak from 423 K to 923 K , coupled with a maximum reduction peak centered at 813 K , which was consistent with the literature report [39]. It was probably that the In_2O_3 evenly distributed on the surface was preferentially reduced at lower temperature, and the bulk In_2O_3 was reduced at higher temperature. However, 9Cu1In/SBA-15 displayed two distinct adjacent hydrogen consumption peaks with nearly the same peak height. The first peak was at the same position with that of 10Cu/SBA-15, while the second one appeared at higher temperature of 484 K , and no hydrogen consumption peak was detected at higher temperature. With the increase of indium content, only the reduction peak at 484 K was observed for 4Cu6In/SBA-15. These results indicated that the existence of copper could promote the reduction of indium oxide. Besides the homogeneously dispersed copper species described in 10Cu/SBA-15, another reducible copper species might be formed with a strong chemical interaction with indium compounds, and this new phase was already

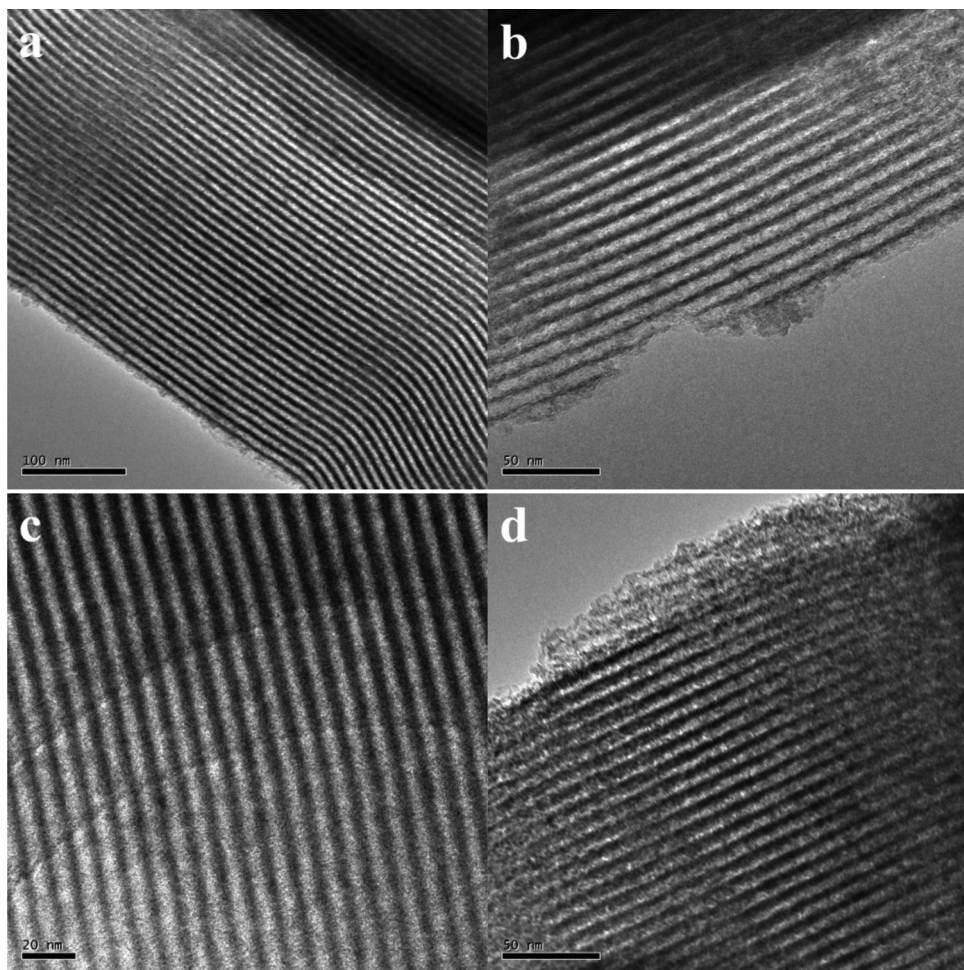


Fig. 3. TEM images of SBA-15 and the reduced catalysts: (a) SBA-15, (b) 10Cu/SBA-15, (c) 9Cu1In/SBA-15 and (d) 10In/SBA-15.

proved to be copper-indium alloy by XRD patterns [26].

Another H₂-TPR process was conducted after the reduced sample was treated in N₂O flow. As shown in Fig. 4B, the sharp peak at 426 K was ascribed to the reduction of Cu₂O on the surface of bulk copper. As for 10Cu/SBA-15, the Cu₂O reduction peak shifted to a lower temperature of 403 K, mainly because that the dispersion of copper over SBA-15 could greatly enhance its reducibility. The H₂-TPR profile of 10In/SBA-15 exhibited a broad reduction peak of In₂O₃ with a much lower intensity between 750 and 960 K, indicating the oxidation of metallic indium during the N₂O chemisorption. Individual peak of Cu₂O could also be observed at 410 K in the curve of 9Cu1In/SBA-15 and 4Cu6In/SBA-15. In addition, there was a distinct peak centered at 645 K for 4Cu6In/SBA-15, which might be ascribed to the reduction In₂O₃, and the reduction of In₂O₃ to metallic In might be much easier in the presence of Cu₂O. Due to the low content of indium, no In₂O₃ reduction peak was observed for 9Cu1In/SBA-15.

3.5. XPS

XPS was employed to investigate the chemical state and composition of surface species on the reduced 10Cu/SBA-15 and 9Cu1In/SBA-15 samples. As shown in Fig. 5, Cu 2p spectra exhibited two significant peaks resulted from orbital spin splitting, which were assigned to Cu 2p_{3/2} and Cu 2p_{1/2} peaks, respectively. Neither of 10Cu/SBA-15 and 9Cu1In/SBA-15 showed observable Cu 2p satellite peak in the range from 942 eV to 944 eV, implying the completely reduction of Cu²⁺ species [40]. However, there was a minor difference between the Cu 2p binding energy of 10Cu/SBA-15 and 9Cu1In/SBA-15. The Cu 2p_{3/2} and

Cu 2p_{1/2} peaks of 10Cu/SBA-15 were centered at the binding energy of 933.1 eV and 952.8 eV, respectively. While Cu 2p_{3/2} and Cu 2p_{1/2} peaks in 9Cu1In/SBA-15 were somewhat shifted, and were 0.1 eV lower than those in 10Cu/SBA-15, located at the binding energy of 933.0 eV and 952.7 eV, respectively. Similarly, it was also reported that Cu 2p_{3/2} peak of CuInS₂ films was centered at 933.0 eV [41]. These results demonstrated the interaction between copper and indium species. As the electronegativity of copper (1.9) was higher than that of indium (1.7), it was assumed that the electron donation from the In atom to the incompletely filled s-band of Cu was more likely to occur, bringing about a decrease in copper 2p electron binding energy. This supposition has been certified by theoretical calculation. Liu et al. [31] found that In atoms acted as electron donors in Cu₂In (100) planes, and 0.33 |e| was transferred to the Cu atoms from In atoms, resulting in a relatively stronger intermediates adsorption strength on Cu atoms of Cu₂In (100). Considering that there was no prominent difference between Cu 2p_{3/2} and Cu 2p_{1/2} of Cu⁺ and Cu⁰ species [42], chemical state differentiation could be difficult with XPS only. However, it was worth noting that the existence of Cu⁰ species was proved by XRD characterization on the reduced catalyst samples and the used catalysts. Analogously, with the help of XAES, Chen et.al [38] also found that the Cu⁰ species predominated on Cu/SBA-15 which was prepared by the deposition precipitation method described in this article. In summary, the Cu species were mainly in the form of metallic copper, which was assumed to have an important role in the activation of hydrogen.

In addition, the XPS characterization also provided useful information on the surface distribution of In and Cu atoms. The contents of Cu and In on the surface of 9Cu1In/SBA-15 were 7.64 wt% and

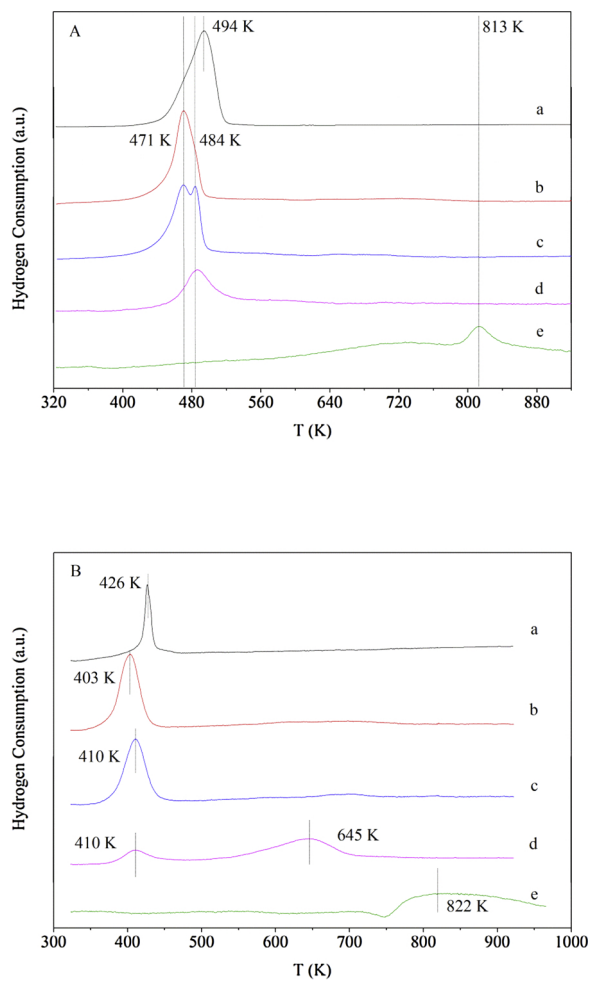


Fig. 4. H₂-TPR profiles of the representative samples (A) calcined in air and (B) treated in N₂O flow: (a) bulk CuO, (b) 10Cu/SBA-15, (c) 9Cu1In/SBA-15, (d) 4Cu6In/SBA-15 and (e) 10In/SBA-15.

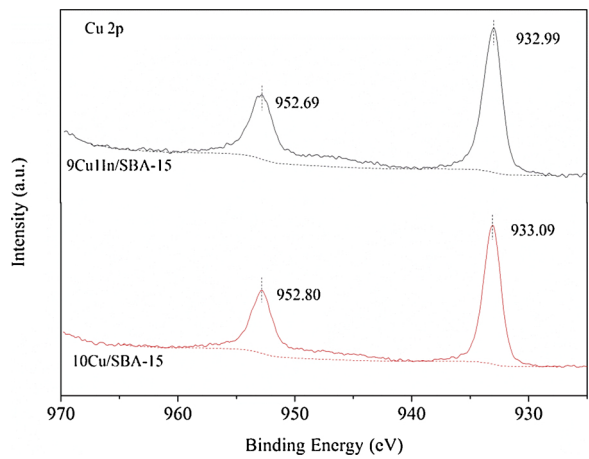


Fig. 5. Cu 2p XPS spectra of the reduced (a) 10Cu/SBA-15 and (b) 9Cu1In/SBA-15.

1.17 wt%, respectively. However, the contents of Cu and In in the bulk phase obtained by ICP were 8.59 wt% and 0.53 wt%, respectively (shown in Table 2). The weight ratio of In/Cu on the surface of catalyst (0.153) was more than twice that in the bulk phase (0.062), strongly suggesting that indium species tended to migrate and enriched on the surface of catalysts.

3.6. H₂ chemisorption

The H₂ chemisorption over monometallic and bimetallic catalysts was evaluated by static volumetric adsorption technique at 77 K. Neither parent SBA-15 nor 10In/SBA-15 could chemisorb H₂, but the loading of copper onto SBA-15 afforded an irreversible hydrogen uptake. Meanwhile, it was worth noting that hydrogen could be adsorbed on both Cu-In alloy and metallic Cu sites, but the exact amount of hydrogen that adsorbed on metallic copper or Cu-In alloy sites was indeed difficult to be identified and calculated by our current characterization methods. Therefore, the amount of hydrogen chemisorbed on the Cu-In bimetallic catalysts was provided. The amount of H₂ uptake for 10Cu/SBA-15 was 126 $\mu\text{mol g}^{-1}$. In general, the hydrogen adsorption amount was positively correlated with the active copper surface area calculated from N₂O chemisorption. In addition, the indium doping also slightly improved the hydrogen adsorption capacity of copper. As shown in Table 2, the maximum amount of H₂ uptake was 149 $\mu\text{mol g}^{-1}$ for 9.5Cu0.5In/SBA-15. With the continuous decrease of copper loading, the H₂ uptake of the bimetallic catalysts reduced gradually. However, the amount of H₂ uptake was far below the amount of surface copper species. It was reported that H₂ chemisorption on metallic copper surface was much lower than the saturated monolayer adsorption, and only some special Cu sites were capable of strongly anchoring H₂ [42].

3.7. N₂O chemisorption

The chemisorption of N₂O was conducted to identify the dispersion of copper on SBA-15, as complement to XRD and TEM. The hydrogen consumption for Cu₂O reduction was obtained by the integration of peak at around 405 K in the H₂-TPR profile after N₂O chemisorption (shown in Fig. 4B), excluding the contribution from the reduction of In₂O₃. The copper dispersion, exposed copper surface area and the average volume-surface diameter were calculated and summarized in Table 2. It could be found that the calculated copper surface area was linearly correlated to the copper content, and varied between 3.4 $\text{m}^2/\text{(g-cat.)}$ and 41.3 $\text{m}^2/\text{(g-cat.)}$. What's more, the hydrogen adsorption capacity was closely correlated to the amount of metallic copper sites, and the larger copper surface area was favorable for promoting hydrogen adsorption capacity.

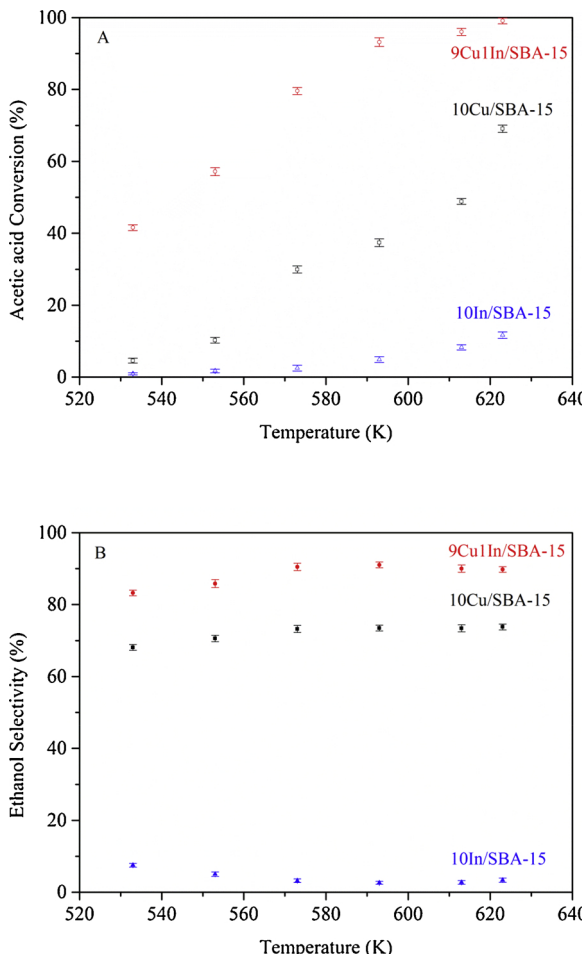
Previous studies showed that the copper dispersion was generally negatively correlated with copper content for supported copper catalysts [43–47]. As shown in Table 2, the three samples (10Cu/SBA-15, 9.5Cu0.5In/SBA-15 and 9Cu1In/SBA-15) with Cu loading around 9% exhibited similar copper dispersion degrees (~67%), while the 8Cu2In/SBA-15 sample with lower copper content possessed higher copper dispersion (74.1%). However, for the other samples with higher nominal In/(Cu + In) weight ratios (> 0.2), the dispersion degree of copper species became lower as the copper content decreased. It was speculated that indium doping was detrimental to the dispersion of copper species, and excessive indium species might hinder the accessibility to copper, thus significantly inhibiting the copper dispersion.

3.8. Catalytic performance evaluation

Preliminary catalytic performance evaluation was conducted to quantify the significant promotion of catalytic activity brought by indium doping. It was found that copper was inactive in C–C bond cleavage, which was the dominant process of carboxylic acid hydrogenation over some monometallic catalysts, including noble metals and nickel ones. The main products of acetic acid hydrogenation over 10Cu/SBA-15 were mainly ethanol, ethyl acetate, and acetaldehyde. Besides, trace amounts of acetone, CO₂, and diethyl ether could also be detected. Fig. 6 displayed that the acetic acid conversion and ethanol selectivity on monometallic and bimetallic catalysts as a function of temperature, other reaction conditions were fixed at pressure of 2.5 MPa, LHSV of 1.25 h^{-1} and n (H₂)/n (AcOH) molar ratio of 30. As reaction

Table 2The catalyst compositions, active copper surface area and dispersion, irreversible H_2 uptake for $xCu_{yIn}/SBA-15$.

Catalyst	Composition (wt%) ^a		Copper surface area (m^2/g cat.) ^b	Copper dispersion (%) ^b	d_{Cu} (nm) ^b	Irreversible H_2 uptake at 77 K ($\mu\text{mol/g}$ cat.)	STY (mg/(ml-cat. h)) ^c
	Cu	In					
10Cu/SBA-15	9.34	–	41.3	68.7	1.5	126	410
9.5Cu0.5In/SBA-15	9.11	0.34	38.7	66.1	1.5	149	642
9Cu1In/SBA-15	8.59	0.53	38.1	68.9	1.5	131	714
8Cu2In/SBA-15	7.78	1.49	37.1	74.1	1.3	83	677
6Cu4In/SBA-15	6.13	2.61	19.8	50.1	2.0	62	651
4Cu6In/SBA-15	4.16	4.84	8.2	30.7	3.3	61	609
2Cu8In/SBA-15	1.90	7.10	3.4	27.5	3.6	33	344
10In/SBA-15	–	8.56	–	–	–	–	3

^a Metal compositions determined by ICP-OES.^b Calculated from N_2O chemisorption.^c $p = 2.5 \text{ MPa}$, LHSV = 1.25 h^{-1} .**Fig. 6.** Effect of reaction temperature on the (A) conversion of acetic acid and (B) ethanol selectivity for mono- and bi-metallic catalysts (Reaction condition: pressure = 2.5 MPa , $n(H_2)/n(AcOH) = 30$, LHSV = 1.25 h^{-1}).

temperature increased from 533 K to 623 K, the conversion of acetic acid over 10Cu/SBA-15 increased dramatically from 4.6% to 69.1%, while the selectivity of ethanol rose slightly from 68% to 73% at 573 K, then remained unchanged in the temperature range between 573 K and 623 K. The supported indium catalyst showed extremely poor catalytic activity for acetic acid hydrogenation, the maximum conversion of acetic acid over 10In/SBA-15 was only 11.7%, with corresponding low ethanol selectivity of 3.4%. It was probably because that hydrogen could not dissociate on the surface of indium species, as evidenced by H_2 chemisorption in Section 3.6. In addition, DFT studies also showed

that indium was chemically inert in this reaction system, and only copper acted as the active site [31], fitting well with the experimental result in present work.

However, the bimetallic 9Cu1In/SBA-15, which owned slightly lower metallic copper surface area and dispersion degree than the monometallic 10Cu/SBA-15, displayed extraordinary hydrogenation performance, especially ethanol selectivity. This fact indicated that the metallic copper surface area was not the sole key factor in determining the acetic acid hydrogenation activity of bimetallic $xCu_{yIn}/SBA-15$ catalysts. The influence of reaction temperature on catalytic performance was coincident with that observed for 10Cu/SBA-15, and the conversion of acetic acid reached 99.1% at 623 K. However, the improvement of acetic acid conversion brought by continuously increasing temperature was not significant. On the contrary, C-C bond cleavage of acetic acid and dehydration of ethanol was more likely to occur at temperature above 630 K, causing a decrease of ethanol selectivity and yield. And the stability of catalyst also got worse at higher temperature. In the previous theoretical simulation calculations of our group, it was found that the addition of indium could modify the properties of copper, and thus significantly reduce the activation barrier of acetate formation from 0.80 eV to 0.37 eV [31,48], which could be accounted for the remarkable improvement of acetic acid conversion on the bimetallic Cu-In catalysts. The *in-situ* DRIFTS characterization on acetic acid hydrogenation in Section 3.10 could also verify this explanation.

What's more, with the introduction of indium, the production of ethyl acetate was sharply suppressed, while the selectivity of intermediate product acetaldehyde showed only little variation, maintaining at around 3%. Meanwhile, the selectivity of ethanol over 9Cu1In/SBA-15 was approximately 15% higher than that on 10Cu/SBA-15, reaching a maximal plateau of 90.5% at the temperature higher than 573 K. According to the previously proposed reaction network for acetic acid hydrogenation, acetaldehyde could be further hydrogenated to ethoxy species, and both ethanol and ethyl acetate were derived from ethoxy species, following two competing pathways: $\text{CH}_3\text{CH}_2\text{O} + \text{H} \rightarrow \text{CH}_3\text{CH}_2\text{OH}$ and $\text{CH}_3\text{CH}_2\text{O} + \text{CH}_3\text{CO} \rightarrow \text{CH}_3\text{COOC}_2\text{H}_5$, respectively. The formation of copper-indium alloy slightly reduced the activation barrier of ethanol formation from 1.43 eV to 1.36 eV, while the activation barrier of ethyl acetate formation dramatically increased from 0.58 eV to 1.02 eV, mainly due to the steric effect of indium in CuIn alloy [31,48]. Therefore, the production of ethyl acetate was greatly inhibited, thus enhancing the selectivity of ethanol.

Fig. 7 displayed the effect of H_2/AcOH molar ratio on acetic acid conversion and selectivity of the main products (ethanol, ethyl acetate and acetaldehyde) over 9Cu1In/SBA-15. The catalytic activity was evaluated under the conditions of 623 K, 2.5 MPa and LHSV of 1.25 h^{-1} . It was observed that the acetic acid conversion was virtually unaffected by changes in molar ratio and always remained at around 99%, indicating that the adsorption and activation of acetic acid was not

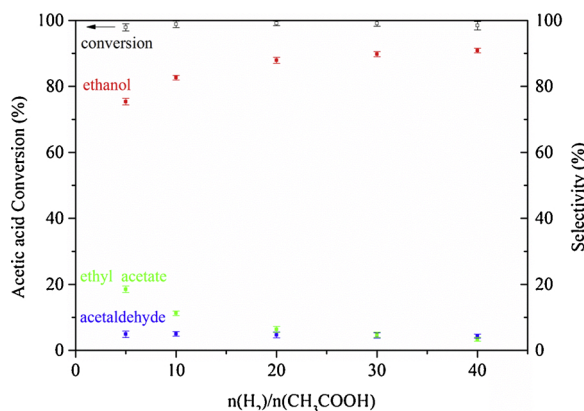


Fig. 7. Effect of $n(H_2)/n(AcOH)$ molar ratio on catalytic performance of 9Cu1In/SBA-15 (Reaction condition: temperature = 623 K, pressure = 2.5 MPa, LHSV = 1.25 h^{-1}).

necessarily related to hydrogen partial pressure under such reaction conditions. With the increase of $H_2/AcOH$ molar ratio from 5 to 40, the ethanol selectivity increased from 75.4% to 90.9%, while the ethyl acetate selectivity decreased accordingly from 18.5% to 3.4%. However, the sum of selectivity of ethanol and ethyl acetate was nearly unchanged and maintained stable at around 94%. In addition, the selectivity of acetaldehyde also maintained constant at around 4.5%. Similar effect of $H_2/AcOH$ molar ratio on the activity was also observed for other catalysts. Therefore, it was speculated that acetic acid was first hydrogenated to form acetaldehyde as an intermediate product, then the acetaldehyde might be further hydrogenated to produce ethoxy species. The higher the partial pressure of hydrogen, the more favorable the consecutive hydrogenation process to produce ethanol, otherwise it was beneficial to generate byproduct ethyl acetate.

In order to further demonstrate the role of indium, the catalytic hydrogenation performance of acetic acid over the CuIn-based catalysts with fixed metal loading but different $In/(Cu + In)$ weight ratios were investigated. The conversion of acetic acid and the selectivity of main products as a function of $In/(Cu + In)$ weight ratio were illustrated in Fig. 8. The reaction conditions were fixed at 623 K, 2.5 MPa, LHSV = 1.25 h^{-1} and $n(H_2)/n(AcOH) = 30$. It was found that as the indium content increased, the acetic acid conversion increased firstly and reached the maximum value of 99.1% for 9Cu1In/SBA-15, then stayed around 98% until the $In/(Cu + In)$ weight ratio reached 0.6, finally downed to 11.7% for 10In/SBA-15. The ethanol selectivity displayed a volcano trend, where the optimal $In/(Cu + In)$ weight ratio was 0.1. Meanwhile, the selectivity of both acetaldehyde and ethyl acetate

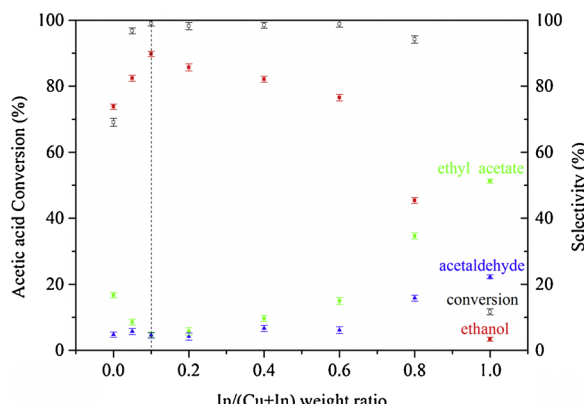


Fig. 8. Acetic acid conversion and selectivity of main products for $xCu1In/SBA-15$ with different $In/(Cu + In)$ weight ratio (Reaction condition: temperature = 623 K, pressure = 2.5 MPa, $n(H_2)/n(AcOH) = 30$, LHSV = 1.25 h^{-1}).

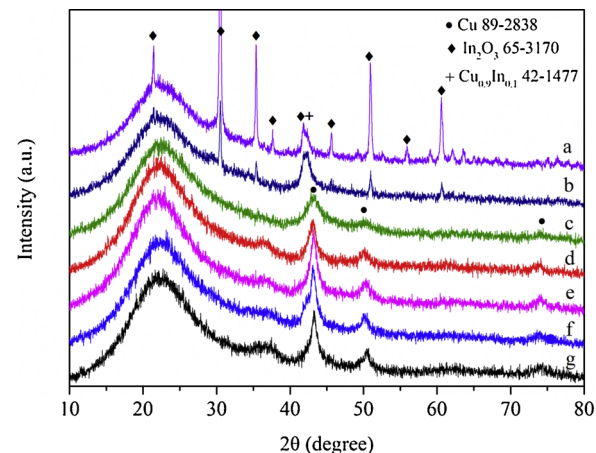


Fig. 9. XRD patterns of the sample after catalytic evaluation: (a) 2Cu8In/SBA-15, (b) 4Cu6In/SBA-15, (c) 6Cu4In/SBA-15, (d) 8Cu2In/SBA-15, (e) 9Cu1In/SBA-15, (f) 9.5Cu0.5In/SBA-15 and (g) 10Cu/SBA-15.

displayed a concave trend, reaching the minimum when $In/(Cu + In)$ was 0.1. Therefore, it seemed that appropriate ratio of copper to indium was essential to obtain high ethanol selectivity.

The space-time yield (STY) of Cu-In bimetallic catalysts were calculated and summarized in Table 2. It was found that the excellent catalytic performance of 9Cu1In/SBA-15 approached or even exceeded that of the precious metal catalysts (Pt or Ru) reported in the literatures [8,9,17,49–52].

3.9. XRD patterns of catalysts after catalytic activity evaluation

In order to confirm the exact phase of active metal species during the reaction process, XRD analysis was conducted immediately after the evaluation of catalytic activity. The diffraction patterns of catalysts with different $In/(Cu + In)$ weight ratios were presented in Fig. 9. The 2Cu8In/SBA-15 exhibited an intense crystalline phase of In_2O_3 , peaks at 2θ of 21.4, 30.5, 35.4, 41.8, 50.9 and 60.6° were assigned to (211), (222), (400), (332), (440) and (622) crystal planes of In_2O_3 phase (JCPDS 65-3170). And besides diffraction peaks of In_2O_3 , a relatively weak peak ascribed to $Cu_{0.9}In_{0.1}$ (111) plane appeared at 2θ of 42.4°, merging together with the (332) plane of In_2O_3 into a relative broad peak. These results indicated that the existence of copper might accelerate the reduction of indium oxide, leading to the formation of Cu-In alloy species during the reaction process. The excess indium species tended to agglomerate into large particles due to its higher mobility above the melting point (439.5 K) than copper atoms. When the temperature was cooled down to ambient condition, the agglomerated In particles was readily converted to oxide [28,29]. With the decrease of $In/(Cu + In)$ weight ratio, the diffraction line intensity of In_2O_3 and $Cu_{0.9}In_{0.1}$ weakened gradually, while the characteristic diffraction peaks of metallic copper phase became much more observable, and they were the only phase detected on the samples where $In/(Cu + In)$ weight ratio was less than 0.6. The In/Cu weight ratio on the surface of the most active catalyst 9Cu1In/SBA-15 obtained by XPS data was 0.15, slightly lower than that of $Cu_{0.9}In_{0.1}$ phase (0.20). Combined with the research of Gyorgy onyestyak et al. [26], it was proposed that indium species tended to enrich on the surface and form Cu-In alloy with part of metallic copper, while the remaining copper was likely to agglomerate into larger particles. Cu-In alloy and Cu might coexisted on the surface of the catalysts, although these two phases couldn't be always detected as the content was too low to reach the detection limit of X-ray diffractometer.

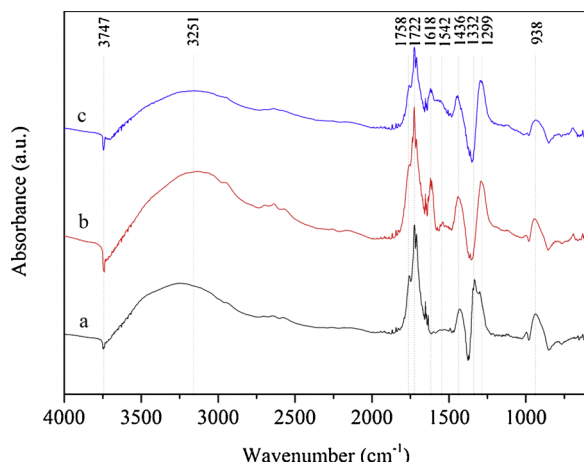


Fig. 10. DRIFT spectra of acetic acid adsorption on (a) SBA-15, (b) 10Cu/SBA-15 and (c) 9Cu1In/SBA-15 at 303 K.

3.10. In-situ DRIFTS of acetic acid adsorption and hydrogenation

The infrared spectra of surface species formed after acetic acid adsorption at 303 K over the SBA-15 and reduced metallic catalysts were illustrated in Fig. 10. The identification of surface species was essential to get insight into the mechanism of acetic acid hydrogenation. Three different surface species could be distinguished when acetic acid was adsorbed on SBA-15, including adsorbed molecular acetic acid, silyl ester and acetate species. The broad absorption band at 3251 cm^{-1} demonstrated that the molecular acetic acid was mainly bonded to the surface of SBA-15 in form of top geometry via hydrogen bonding, which was derived from the interaction between the hydroxyl hydrogen atom on the SBA-15 surface and the lone electron pair on the carbonyl oxygen atom in acetic acid [53,54]. And the characteristic band at 1722 cm^{-1} could be ascribed to the ν (C=O) stretching of this kind of adsorbed acetic acid [17]. In addition, the hydrogen bond caused the disappearance of hydroxyl groups on the surface of SAB-15, resulting in the formation of a distinct negative peak at 3747 cm^{-1} [17]. The infrared absorption bands at 938 cm^{-1} and 1299 cm^{-1} were ascribed to γ (O–H) and ν (C–OH), respectively [53,55]. The absorption peak at 1332 cm^{-1} overlapped with the peak at 1299 cm^{-1} , could be attributed to the deformation vibration of C–H bond [56]. The silyl ester species originated from dissociative acetic acid adsorption on SBA-15 surface showed a C=O stretching vibration absorption band at 1758 cm^{-1} , with relatively low intensity when compared with that of hydrogen bonded acetic acid at 1722 cm^{-1} [53]. The symmetric stretching absorption band of the COO group was observed at 1436 cm^{-1} , confirming the existence of acetate species [55]. However, the asymmetric stretching absorption of COO group, expected around (1500–1600 cm^{-1}), was not reflected in the spectrum, which inferred that acetate adsorbate was existed through the two carboxylate oxygen atoms toward to the surface [57].

Besides the infrared characteristic peaks of acetic acid adsorbed on SBA-15 described above (δ (C–H) not included), some new absorption peaks appeared in the spectra of both 10Cu/SBA-15 and 9Cu1In/SBA-15. The distinct peak at 1618 cm^{-1} could be ascribed to ν (C=O) of adsorbed acetyl species, implying that a part of adsorbed acetic acid was transformed to acetyl in the presence of metal through breaking C–O bond [17,55]. Meanwhile, the absorption peak intensity for acetyl species on 10Cu/SBA-15 was almost identical to that on 9Cu1In/SBA-15, because the activation barrier for C–O bond scission on Cu(111) plane (1.43 eV) was rather close to that on Cu2In(100) plane (1.36 eV) [31,48]. The shoulder at 1542 cm^{-1} was assigned to asymmetric ν_a (COO) stretching [53,54,58,59]. However, the absorption peak intensity for ν_a (COO) on 10Cu/SBA-15 was far below that on 9Cu1In/

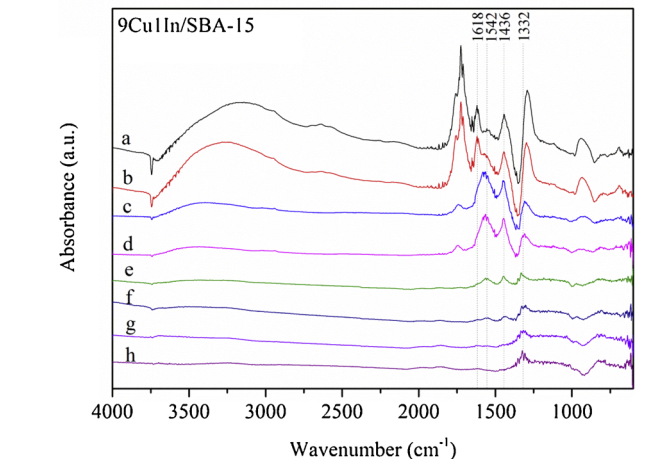
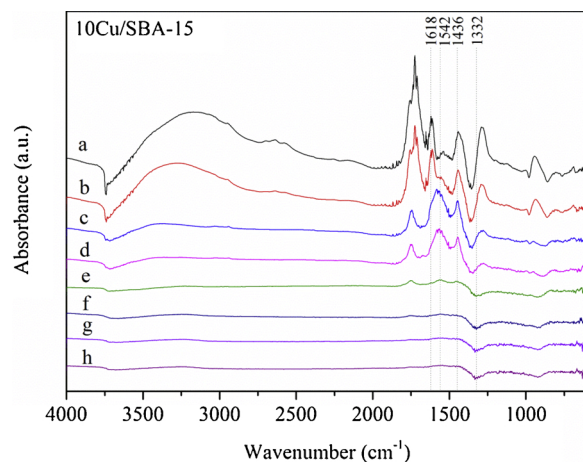
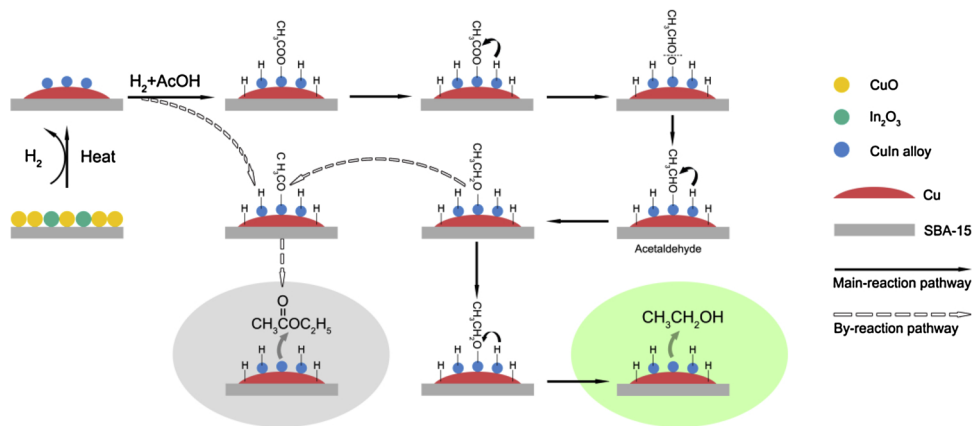


Fig. 11. In-situ DRIFTS spectra of acetic acid hydrogenation on 10Cu/SBA-15 and 9Cu1In/SBA-15 at different temperature: (a) 303 K, (b) 323 K, (c) 373 K, (d) 423 K, (e) 473 K, (f) 523 K, (g) 573 K, (h) 623 K.

SBA-15, indicating that acetic acid dissociation through O–H bond cleavage was more likely to occur on 9Cu1In/SBA-15. Interestingly, according to the previous simulation work in our group, the indium doping on copper could significantly lower the activation barrier for the formation of acetate species, which could be taken as further evidence of the experimental results in this work. And the calculated activation barrier for this elementary step on Cu(111) and Cu₂In(100) planes were 0.80 eV and 0.37 eV, respectively [31,48].

Fig. 11 displayed in-situ DRIFTS spectra of acetic acid hydrogenation following stepwise heating. The characteristic IR absorption bands of acetic acid adsorbed on 10Cu/SBA-15 and 9Cu1In/SBA-15 at 303 K were discussed in former section, the molecular acetic acid and silyl ester were mainly adsorbed on the surface of SBA-15. After the introduction of H₂ into the system, as the temperature increased from 303 K to 423 K, the intensities of absorption peak at 1542 cm^{-1} and 1436 cm^{-1} , corresponding to ν_a (COO) and ν_s (COO), increased progressively, while other absorption peaks belonging to the adsorbed molecular acetic acid, acetyl species, and silyl ester were gradually weakened with temperature increasing, and those for acetyl species even disappeared at 373 K, which was far below the temperature required for acetic acid hydrogenation. Combining with Willy Rachmady *et al.*'s research on acetic acid reduction over iron catalysts, it was speculated that neither molecularly adsorbed acetic acid nor silyl ester participated in the hydrogenation process on copper catalysts, the acetyl species hydrogenation seemed to be impossible under the



Scheme 1. Schematic diagram of acetic acid hydrogenation on Cu-In bimetallic catalyst.

reaction conditions, and the acetate derived from O–H bond breaking of adsorbed acetic acid or silyl ester decomposition was most likely to serve as the active intermediate species [53].

Furthermore, a new peak attributable to δ (CH) emerged at 1332 cm^{-1} in the spectra of 9Cu1In/SBA-15 when the temperature rose above 373 K, manifesting that acetate species could be further hydrogenated to form dioxyethylidene over 9Cu1In/SBA-15. This phenomenon was in line with the most favorable route to produce ethanol from acetic acid reduction on the Cu₂In(100) surface, which was proposed in our earlier work. It was demonstrated that acetaldehyde, as a wide accepted intermediate product of acetic acid hydrogenation, was produced mainly following the optimal pathway: $\text{CH}_3\text{COOH} \rightarrow \text{CH}_3\text{COO} \rightarrow \text{CH}_3\text{CHOO} \rightarrow \text{CH}_3\text{CHO}$, with dioxyethylidene formation serving as the rate-limiting step [31]. Then, the formed acetaldehyde could be further hydrogenated to ethanol. However, as there was no peak ascribed to δ (CH) observed in the spectra of 10Cu/SBA-15, the transformation from acetate to dioxyethylidene seemed much more difficult to occur on the copper surface, which might be regarded as one of the reasons for the low activity of monometallic copper catalyst.

3.11. Mechanism of acetic acid hydrogenation on bimetallic Cu-In/SBA-15

In summary, the remarkable promotional effect of indium addition might be attributed to the existence of Cu-In alloy on the surface of catalysts, and the electronic properties of copper was thus changed, which were evidenced by XRD and XPS characterizations. Combining with the experimental results and previous DFT calculations on the acetic acid hydrogenation over Cu(111) and Cu₂In(100) planes [31,48], the possible mechanism of acetic acid hydrogenation over Cu-In bimetallic catalyst was proposed, as shown in **Scheme 1**.

It was proposed that indium species tended to enrich on the surface of support and form Cu-In alloy with part of the metallic copper, while the remaining metallic copper tended to agglomerate into larger particles during the reduction process. Cu-In alloy and metallic Cu coexisted on the surface of the catalysts. Hydrogen was dissociated on both isolated active copper sites and alloyed copper sites, and the concentration of adsorbed hydrogen atoms was one of the key factors that determine the selectivity of ethanol. While the acetic acid dissociation to acetate species was dominant on the alloyed copper active sites, following the reaction pathway: $\text{CH}_3\text{COOH} \rightarrow \text{CH}_3\text{COO} + \text{H}$. And there were also some acetyl species formed through breaking of C–OH bond, but with more difficulty than the formation of acetate. When compared with monometallic copper, copper-indium alloy could significantly reduce the difficulty of acetate formation, thereby promoting the catalytic conversion of acetic acid to ethanol.

Next, the as formed acetate species was transformed to acetaldehyde through hydrogenation and deoxygenation in sequence. As an intermediate product, acetaldehyde was further hydrogenated to form

ethoxy species. The consumption of ethoxy species might take place along two competing pathways: ethoxy species could combine with a hydrogen atom or an acetyl group, producing ethanol and ethyl acetate, respectively. However, the formation of ethyl acetate would be greatly suppressed due to the block effect of indium in Cu-In alloy, thus realizing the improvement of ethanol selectivity to some extent.

4. Conclusions

In the present work, the highly efficient bimetallic CuIn/SBA-15 catalyst was prepared by deposition precipitation method and applied for the synthesis of ethanol via acetic acid hydrogenation. A series of physicochemical characterizations were conducted to validate and refine the previously proposed mechanism for this reaction system: $\text{CH}_3\text{COOH} \rightarrow \text{CH}_3\text{COO} \rightarrow \text{CH}_3\text{CHOO} \rightarrow \text{CH}_3\text{CHO} \rightarrow \text{CH}_3\text{CH}_2\text{O} \rightarrow \text{CH}_3\text{CH}_2\text{OH}$. Besides low price, the most prominent advantage of copper catalyst over noble metal catalysts was its inherent inertness of C–C bond hydrogenolysis, which restrained the production of CH_4 and CO. With the introduction of indium, the catalytic activity and the selectivity toward ethanol was significantly enhanced, mainly due to the synergy inside Cu-In alloy phase. On the copper-indium alloy sites, the difficulty of acetic acid dissociation to acetate was significantly reduced, promoting the conversion of acetic acid to acetaldehyde. Meanwhile, the ethyl acetate formation via combination of acetyl and ethoxy was inhibited to some extent due to the steric hindrance effect of the indium atoms. In addition, the concentration of dissociated hydrogen atoms adsorbed on the catalyst surface, which was associated with the copper surface area and H_2 partial pressure, was one of pivotal factors affecting the selectivity of ethanol. Notably, the optimal catalytic activity was obtained over 9Cu1In/SBA-15, where acetic acid conversion and ethanol selectivity reached 99.1% and 90.9%, respectively. Based on the above results, the novel bimetallic copper-indium catalyst was expected to be applied for the acetic acid hydrogenation to synthesis ethanol, thus replacing noble metal catalysts.

Acknowledgments

This work was financially supported by the National Natural Science Foundation of China (No. 21406159).

References

- [1] V. Subramani, S.K. Gangwal, *Energy Fuels* 22 (2008) 814–839.
- [2] V.J. Johnston, L. Chen, B.F. Kimmich, J.T. Chapman, J.H. Zink, H. Weiner, J.L. Potts, R. Jevtic, *Catalysts for Making Ethanol From Acetic Acid*, WO, 2013.
- [3] G.J. Sunley, D.J. Watson, *Catal. Today* 58 (2000) 293–307.
- [4] N. Yoneda, S. Kusano, M. Yasui, P. Pujado, S. Wilcher, *Appl. Catal. A-Gen.* 221 (2001) 253–265.
- [5] H. Weiner, Z. Zhou, V.J. Johnson, *Process for Producing Ethanol with Zonal*

Catalysts, (2016).

[6] G. Onyestiyak, S. Harnos, C.A. Badari, E. Drotar, S. Klebert, D. Kallo, *Open Chem.* 13 (2015) 517–527.

[7] R. Alcala, J.W. Shabaker, G.W. Huber, M.A. Sanchez-Castillo, J.A. Dumesic, *J. Phys. Chem. B* 109 (2005) 2074–2085.

[8] K. Zhang, H. Zhang, H. Ma, W. Ying, D. Fang, *Catal. Lett.* 144 (2014) 691–701.

[9] S. Zhang, X. Duan, L. Ye, H. Lin, Z. Xie, Y. Yuan, *Catal. Today* 215 (2013) 260–266.

[10] W. Rachmady, M.A. Vannice, *J. Catal.* 192 (2000) 322–334.

[11] W. Rachmady, M.A. Vannice, *J. Catal.* 209 (2002) 87–98.

[12] V. Pallassana, M. Neurock, *J. Catal.* 209 (2002) 289–305.

[13] H. Olcay, Y. Xu, G.W. Huber, *Green Chem.* 16 (2014) 911–924.

[14] L. Chen, Y. Zhu, H. Zheng, C. Zhang, B. Zhang, Y. Li, *J. Mol. Catal. A-Chem.* 351 (2011) 217–227.

[15] J. Shangguan, M.V. Olarte, Y.-H. Chin, *J. Catal.* 340 (2016) 107–121.

[16] Y. Ito, H. Kawamoto, S. Saka, *Fuel* 178 (2016) 118–123.

[17] M. Zhou, H. Zhang, H. Ma, W. Ying, *Fuel* 203 (2017) 774–780.

[18] H. Olcay, L. Xu, Y. Xu, G.W. Huber, *Chemcatchem* 2 (2010) 1420–1424.

[19] M. Zhang, R. Yao, H. Jiang, G. Li, Y. Chen, *RSC Adv.* 7 (2017) 1443–1452.

[20] M. Luo, T.K. Das, C. Delibas, B.H. Davis, *Top. Catal.* 57 (2014) 757–761.

[21] S. Wang, W. Guo, H. Wang, L. Zhu, S. Yin, K. Qiu, *New J. Chem.* 38 (2014) 2792–2800.

[22] M.A.N. Santiago, M.A. Sanchez-Castillo, R.D. Cortright, J.A. Dumesic, *J. Catal.* 193 (2000) 16–28.

[23] C. Liu, X. Guo, Q. Guo, D. Mao, J. Yu, G. Lu, *J. Mol. Catal. A-Chem.* 425 (2016) 86–93.

[24] A.V.H. Soares, J.B. Salazar, D.D. Falcone, F.A. Vasconcellos, R.J. Davis, F.B. Passos, *J. Mol. Catal. A-Chem.* 415 (2016) 27–36.

[25] N.N. Pandhare, S.M. Pudi, P. Biswas, S. Sinha, *J. Taiwan Inst. Chem. Eng.* 61 (2016) 90–96.

[26] G. Onyestiyak, S. Harnos, S. Klebert, M. Stolcova, A. Kaszonyi, D. Kallo, *Appl. Catal. A-Gen.* 464 (2013) 313–321.

[27] S. Harnos, G. Onyestiyak, R. Barthos, M. Stolcova, A. Kaszonyi, J. Valyon, *Cent. Eur. J. Chem.* 10 (2012) 1954–1962.

[28] S. Harnos, G. Onyestiyak, J. Valyon, *Appl. Catal. A-Gen.* 439 (2012) 31–40.

[29] G. Onyestiyak, S. Harnos, D. Kalló, *Catal. Commun.* 26 (2012) 19–24.

[30] G. Onyestiyák, *Catal. Commun.* 38 (2013) 50–53.

[31] J. Liu, H. Lyu, Y. Chen, G. Li, H. Jiang, M. Zhang, *J. Chem. Soc. Faraday Trans.* 19 (2017) 28083–28097.

[32] A. Chiriac, B. Dragoi, A. Ungureanu, C. Ciotonea, I. Mazilu, S. Royer, A.S. Mamede, E. Rombi, I. Ferino, E. Dumitriu, *J. Catal.* 339 (2016) 270–283.

[33] A.V.-H. Soares, G. Perez, F.B. Passos, *Appl. Catal. B* 185 (2016) 77–87.

[34] C. Van Der Grift, A. Wielers, B. Jogh, J. Van Beunum, M. De Boer, M. Versluijs-Helder, J. Geus, *J. Catal.* 131 (1991) 178–189.

[35] D. Zhao, J. Feng, Q. Huo, N. Melosh, G.H. Fredrickson, B.F. Chmelka, G.D. Stucky, *Science* 279 (1998) 548–552.

[36] P.I. Ravikovitch, A.V. Neimark, *Langmuir* 18 (2002) 9830–9837.

[37] Y. Wang, J. Liao, J. Zhang, S. Wang, Y. Zhao, X. Ma, *Aiche J.* 63 (2017) 2839–2849.

[38] L.-F. Chen, P.-J. Guo, L.-J. Zhu, M.-H. Qiao, W. Shen, H.-L. Xu, K.-N. Fan, *Appl. Catal. A Gen.* 356 (2009) 129–136.

[39] A. Gervasini, J.A. Perdigon-Melon, C. Guimon, A. Auroux, *J. Phys. Chem. B* 110 (2006) 240–249.

[40] J. Gong, H. Yue, Y. Zhao, S. Zhao, L. Zhao, J. Lv, S. Wang, X. Ma, *J. Am. Chem. Soc.* 134 (2012) 13922–13925.

[41] R. Scheer, H. Lewerenz, *J. Vac. Sci. Technol. A: Vac. Surf. Films* 12 (1994) 56–60.

[42] X. Zheng, H. Lin, J. Zheng, H. Ariga, K. Asakura, Y. Yuan, *Top. Catal.* 57 (2014) 1015–1025.

[43] H. Liu, Z. Huang, H. Kang, X. Li, C. Xia, J. Chen, H. Liu, *Appl. Catal. B-Environ.* 220 (2018) 251–263.

[44] D. Vargas-Hernandez, J.M. Rubio-Caballero, J. Santamaria-Gonzalez, R. Moreno-Tost, J.M. Merida-Robles, M.A. Perez-Cruz, A. Jimenez-Lopez, R. Hernandez-Huesca, P. Maireles-Torres, *J. Mol. Catal. A-Chem.* 383 (2014) 106–113.

[45] M. Turco, G. Bagnasco, C. Cammarano, P. Senese, U. Costantino, M. Sisani, *Appl. Catal. B-Environ.* 77 (2007) 46–57.

[46] H. Yan, X.-T. Qin, Y. Yin, Y.-F. Teng, Z. Jin, C.-J. Jia, *Appl. Catal. B-Environ.* 226 (2018) 182–193.

[47] X. Cheng, X. Zhang, D. Su, Z. Wang, J. Chang, C. Ma, *Appl. Catal. B* 239 (2018) 485–501.

[48] M. Zhang, R. Yao, H. Jiang, G. Li, Y. Chen, *Appl. Surf. Sci.* 412 (2017) 342–349.

[49] J. Zhang, J. Luo, J. Gao, D. Liu, *Can. J. Chem. Eng.* 95 (2017) 1109–1116.

[50] K. Zhang, H. Zhang, H. Ma, W. Ying, D. Fang, *Polish J. Chem. Technol.* 17 (2015) 11–17.

[51] P.K. Rakshit, R.K. Voolapalli, S. Upadhyayula, *Mol. Catal.* 448 (2018) 78–90.

[52] M. Zhou, H. Zhang, H. Ma, W. Ying, *Ind. Eng. Chem. Res.* 56 (2017) 8833–8842.

[53] W. Rachmady, M.A. Vannice, *J. Catal.* 208 (2002) 170–179.

[54] M. Hasan, M. Zaki, L. Pasupulety, *Appl. Catal. A Gen.* 243 (2003) 81–92.

[55] W. Rachmady, M.A. Vannice, *J. Catal.* 207 (2002) 317–330.

[56] M. Singh, N. Zhou, D.K. Paul, K.J. Klabunde, *J. Catal.* 260 (2008) 371–379.

[57] S. Beyhan, J.-M. Léger, F. Kadırgan, *Appl. Surf. Sci.* 321 (2014) 426–431.

[58] S. Nishiyama, T. Hara, S. Tsuruya, M. Masai, *J. Phys. Chem. B* 103 (1999) 4431–4439.

[59] Z.-F. Pei, V. Ponec, *Appl. Surf. Sci.* 103 (1996) 171–182.